Biomimetic Peptide−Amphiphiles for Functional Biomaterials: The Role of GRGDSP and PHSRN

Anastasia Mardilovich† and Efrosini Kokkoli*,‡

Department of Chemical Engineering, University of Massachusetts, Amherst, Massachusetts 01003, and Department of Chemical Engineering and Materials Science, University of Minnesota, Minneapolis, Minnesota 55455

Received October 28, 2003; Revised Manuscript Received February 6, 2004

The study we present involves the use of a biomimetic system that allows us to study specific interactions in the $\alpha_5\beta_1$ receptor−GRGDSP ligand system with an atomic force microscope (AFM). Bioartificial membranes that mimic the adhesion domain of the extracellular matrix protein fibronectin are constructed from peptide−amphiphiles. A novel peptide−amphiphile is designed that contains both GRGDSP (Gly-Arg-Gly-Asp-Ser-Pro, the primary recognition site for $\alpha_5\beta_1$) and PHSRN (Pro-His-Ser-Arg-Asn, the synergy binding site for $\alpha_5\beta_1$) sequences in a single peptide formulation, separated by a spacer. Two different antibodies are used to immobilize and activate isolated $\alpha_5\beta_1$ integrins on the AFM tip. The interaction measured between immobilized $\alpha_5\beta_1$ integrins and peptide−amphiphiles is specific for integrin−peptide binding and is affected by divalent cations in a way that accurately mimics the adhesion function of the $\alpha_5\beta_1$ receptor. The strength of the PHSRN synergistic effect depends on the accessibility of this sequence to $\alpha_5\beta_1$ integrins. An increase in adhesion is observed compared to surfaces displaying only GRGDSP peptides when the new biomimetic peptide−amphiphiles are diluted with lipidated poly(ethylene glycol), which provides more space for the peptide headgroups to bend and expose more of the PHSRN at the interface.

Introduction

Cell−matrix adhesion mediated by integrins was shown to regulate aspects of cell behavior such as growth, differentiation, adhesion, and motility.[1−10]

The $\alpha_5\beta_1$ integrin is one of the 24 known members of the integrin family of adhesion molecules, formed by two noncovalently associated α and β subunits. Each subunit consists of an extracellular domain, a transmembrane domain, and a short cytoplasmic tail.[11−12] The current model for structural association of these subunits predicts that integrins exist in two different conformation states: inactive, when they are unable to bind ligand, or active, when they are capable of binding their ligand with high affinity.[13] $\alpha_5\beta_1$ integrins can be activated by indirect stimuli (signaling that acts on the cytoplasmic tail) and direct stimuli, such as anti-β_1 chain monoclonal antibodies (e.g., TS2/16)[14,15] and divalent ions (Mg^{2+} and Mn^{2+}).[16,17] In general, it has been shown that Mn^{2+} activates isolated $\alpha_5\beta_1$ integrins and promotes their high affinity binding to the ligand, whereas Ca^{2+} inhibits ligand binding, and Mg^{2+} plays a stimulatory role but to a lesser extent than Mn^{2+}.[16] Earlier studies of the regulation of $\alpha_5\beta_1$−fibronectin interactions have demonstrated the presence of at least three distinct classes of cation binding sites for Mg^{2+}, Mn^{2+}, and Ca^{2+}.[17] Mn^{2+}-supported binding was strongly inhibited by Ca^{2+} in a noncompetitive manner, suggesting distinct binding sites for these two cations. Another site was found to bind Ca^{2+} and Mg^{2+} in a competitive manner. Both monoclonal antibodies and divalent cations have been used in this work as stimuli to investigate the dynamic regulation of integrin−ligand binding. Purified $\alpha_5\beta_1$ integrins are used in this study to investigate receptor−ligand interactions and avoid any complications associated with real cells, such as membrane diffusion, cell viscoelastic deformation, and receptor/cytosceletal interactions.[18]

Integrins bind to the adhesion domain of the extracellular matrix (ECM) proteins by recognizing specific sites of that domain.[19−21] The prototype for the integrin binding site is the Arg-Gly-Asp (RGD) sequence that is present in fibronectin, fibrinogen, vitronectin, and other adhesive proteins.[19,22] Therefore, peptides containing the RGD sequence have been used extensively to mimic ECM proteins and, thus, to provide biomimetic models to study interactions between cells and their environment.[23−28] Various approaches have been utilized in an attempt to attach cell adhesion peptides to the surfaces.[25,26,29−37] In particular, it has been demonstrated that connecting peptides to synthetic lipid tails allows them to self-assemble into highly organized biomimetic surfaces, which effectively promotes cell adhesion, spreading, migration, growth, and differentiation.[38−46]

In this study, bioartificial membranes, which display peptides that mimic the adhesion domain of the ECM protein fibronectin, are constructed from mixtures of peptide−amphiphiles and poly(ethylene glycol) (PEG) amphiphilic molecules, DSPE-PEG120 [PEG chains with a molecular

* To whom correspondence should be addressed: kokkoli@cems.umn.edu; (612) 626-1185.

† University of Massachusetts. Present address: Department of Chemical Engineering and Materials Science, University of Minnesota.

‡ University of Minnesota.

10.1021/bm0344351 CCC: $27.50
Published on Web 03/13/2004

weight of 120 covalently linked to 1,2-Distearoyl-*sn*-glycero-3-phosphatidylethanolamine (DSPE) are referred to as PEG120 in the remaining of the text]. PEG has been used extensively as material that is nonadhesive to biological molecules[33,46,47] and is utilized here to dilute the surface concentration of the peptide−amphiphile. The peptide−amphiphile structure includes dialkyl ester tails that allow control over their length (C_{16}), a glutamic acid (Glu) linker, a $-(CH_2)_2-$ spacer, and a headgroup that contains the bioactive sequence. The tails serve to align the peptide strands and provide a hydrophobic surface for self-association and interaction with other hydrophobic surfaces.[38] The two peptide sequences used in this study are found in fibronectin: the tenth type III module, GRGDSP (the primary recognition site for $\alpha_5\beta_1$ integrins) and the ninth type III module, PHSRN (the synergy binding site for $\alpha_5\beta_1$). These two sequences are separated by 30−40 Å in fibronectin.[48] Fibronectin was chosen for this study because it is a ligand for $\alpha_5\beta_1$ and because of its importance as an ECM component. It is a prototype cell adhesion protein, which is widely distributed in different types of tissues and is, therefore, a potential ligand for most cell types including fibroblasts, mesenchymal cells, myoblasts, endothelial cells, neutrophils, macrophages, and hepatocytes.[49] Fibronectin plays a critical role in various developmental and homeostatic processes, including embryonic development and wound healing.[50,51]

Previous studies on analogous biomimetic models[52,53] have shown that specific recognition of the immobilized $\alpha_5\beta_1$ receptor was significantly increased for a surface that presented mixtures of the two peptides (GRGDSP and PHSRN) compared to the adhesion measured with surfaces that displayed only GRGDSP. In the past when RGD and PHSRN have been presented in a single peptide formulation, results varied depending on the design. Kao et al.[54] used both RGD and PHSRN sequences in a single peptide formulation and both possible orientations (with RGD sequence at the C terminus and PHSRN at the N terminus and vice versa) with a $(G)_6$ linker between the two bioactive sequences to create biomimetic surfaces. Their results demonstrated the role of the synergy between RGD and PHSRN and the importance of the relative order of the two peptides in supporting macrophage fusion to form foreign body giant cells. The peptide sequence that resembled the native register, PHSRN from the III_9 repeat followed by the RGD from the III_{10} repeat, showed the highest activity. Hojo et al. designed a bivalent PEG hybrid of RGD and PHSRN peptides using an amino acid type poly(ethylene glycol) derivative (aaPEG) to study the importance of spatial arrangement between the two bioactive sequences in promoting cell spreading.[55] They have shown an increase in baby hamster kidney cells' spreading activity on hybrid peptides, containing both PHSRN and RGD bridged by aaPEG (PHSRN-aaPEG-RGD) compared to aaPEG-RGD, which suggests the synergistic effect of PHSRN. Furthermore, Aucoin et al.[56] have not observed an increase in adhesion of corneal cells to surfaces modified with RGDS and PHSRN in a single peptide formulation (PHSRNRGDS) compared to surfaces modified with a combination of RGDS and PHSRN peptides at a 50:50 ratio. This result also supports the idea that the correct distance between the adhesion RGD sequence and its synergy site PHSRN is important in mimicking the adhesion properties of fibronectin.

We have designed a new sequence, $PHSRN(SG)_3$-SGRGDSP (referred to as PHSRN-GRGDSP in the remainder of the text), that contains both the primary and the synergy adhesion-mediating sequences of fibronectin in a single peptide formulation. A linker $(SG)_3S$ is used to link these two bioactive sequences in a specific spatial orientation. The theoretical length of this linker is calculated using two different approaches and was found to be approximately 30 Å, 26 Å when calculated using 3.7 Å per amino acid residue,[57] and 32 Å when calculated using standard bond lengths and angles. Serine (S) and glycine (G) are used here because they are small, uncharged amino acid residues with serine being hydrophilic and glycine hydrophobic. This combination of residues was chosen to avoid complications during the purification of peptide−amphiphiles as well as contributions from the linker into the interactions between $\alpha_5\beta_1$ integrins and the peptide. In addition, analysis of the alignment of the amino acid sequences of the Fibronectin-III (FN-III) domains in FN7-10 (SwissPort Database, sequence FINC_HUMAN PO2751) indicated that the ratio of hydrophilic to hydrophobic residues between PHSRN and GRGDSP is almost 1:1, which provided another motivation for choosing the $(SG)_3S$ combination as a linker between the PHSRN and GRGDSP sequences. Thus, the goal in designing the linker was to mimic as closely as possible the distance and the hydrophilicity between the PHSRN and the GRGDSP sequences in the fibronectin molecule.

Peptide−amphiphiles that contain the new bioactive sequence PHSRN-GRGDSP in the headgroup are synthesized and characterized in this study, and interactions between $\alpha_5\beta_1$ integrins and the new sequence are investigated using an atomic force microscope (AFM).

Materials and Methods

Preparation and Characterization of Bioartificial Membranes. DSPE and PEG120 were obtained from Avanti Polar Lipids, Inc. (Alabaster, AL). $(C_{16})_2$-Glu-C_2-KAbuGRGD-SPAbuK, $(C_{16})_2$-Glu-C_2-PHSRN, $(C_{16})_2$-Glu-C_2-$PHSRN(SG)_3$-SGRGDSP, and $(C_{16})_2$-Glu-C_2-GRGESP were synthesized as described elsewhere.[38] These peptide−amphiphiles will be referred as GRGDSP, PHSRN, PHSRN-GRGDSP, and GRGESP, respectively, in the remainder of the text.

Pure peptide−amphiphiles were dissolved at approximately 1 mg/mL in a 99:1 chloroform/methanol solution and stored at 4 °C. The solution was heated to room temperature prior to use.

The Langmuir−Blodgett (LB) technique was used to create supported bioactive bilayer membranes. LB film depositions were done on a KSV 5000 LB system (KSV Instruments, Helsinki, Finland). All the depositions were done at 41 mN/m, which is well below the collapse pressure of 65 mN/m. The deposition speed for both the up and down strokes was 1 mm/min. Freshly cleaved mica disks of radius 7.5 mm were used as substrates for the supported bilayer membranes. The DSPE layer was deposited first at the

upstroke to make the mica surfaces hydrophobic. The second layer with peptide−amphiphiles was deposited in the down stroke. Transfer ratios for both layers were calculated to be in the range 0.8−1, indicating that monolayers were deposited on mica surfaces with minimal disruption. The resulting supported bilayer membranes were transferred into glass vials under water. Care was taken to avoid exposing the surface to air because they rearrange to form multilayers.[58]

AFM characterization of the LB films was done with a Digital Instruments Nanoscope III system equipped with a fluid cell for tapping mode (Digital Instruments, Santa Barbara, CA). Images were obtained in tapping mode in deionized (DI) water using standard 100-μm V-shaped silicon nitride AFM cantilevers with pyramidal tips (Digital Instruments) of nominal radius 5−40 nm and a nominal spring constant of 0.58 N/m. The amplitude setpoint was kept as high as possible to minimize the influence of sample properties on the topographic contrast.[59]

$\alpha_5\beta_1$ Integrins Immobilization. Purified human $\alpha_5\beta_1$ integrins were purchased from Chemicon International (Temecula, CA) and immobilized according to the protocol by Kokkoli et al.[53] Briefly, the integrins were diluted to 5 μg/mL in solution containing 1 mM $MgCl_2$, 20 mM Tris-HCl at pH 7.5, and 0.1% Triton X-100, aliquoted, and stored at −80 °C. The pH of the above solution was adjusted to 7.3 by adding a 0.1 M NaOH solution. Standard 200-μm V-shaped silicon−nitride AFM cantilevers (NP-S20) were washed with ethanol and then placed under a low-wavelength UV light in the presence of water vapors for 10 min. After cleaning, cantilevers were washed with phosphate-buffered saline (PBS) (Life Technologies, Rockville, MD). Goat antiserum to mouse IgG Fc (Cappel, Aurora, OH) was physically adsorbed on cantilevers by incubating them overnight at 37 °C and 5% CO_2 with IgG at a final antibody concentration of 8 μg/mL in PBS. Cantilevers were then washed with PBS and incubated with purified monoclonal mouse anti-human TS2/16 (anti-β_1) antibody (Endogen, Woburn, MA), 20 μg/mL in PBS, for 3 h at 37 °C and 5% CO_2. After washing with PBS, the cantilevers were incubated with purified human $\alpha_5\beta_1$ integrins at 37 °C and 5% CO_2 for 2.5 h and washed with PBS before used. The activity of the integrins was verified via an enzyme-linked immunosorbent assay test.[52] Force measurements were done immediately after the cantilevers were prepared.

Adhesion Force Measurements. Surface force measurements were performed using a commercial AFM, a Nanoscope III (Digital Instruments, Santa Barbara, CA), in contact mode in a 1 mM $MnCl_2$ solution (unless stated otherwise), at a loading rate defined as the spring constant of the cantilever times the velocity of the piezo of 59.8 nN/s, using standard 200-μm V-shaped silicon nitride AFM cantilevers with pyramidal tips (Digital Instruments) of nominal radius 5−40 nm and nominal spring constants of 0.06 or 0.32 N/m. Data were recorded as the two surfaces, the sample surface and the probe tip, were brought into contact and then pulled apart. The adhesion force or the "pull-off" force is defined as the minimum force required to separate two surfaces. All adhesion force measurements were carried out at room temperature and at a pH of the $MnCl_2$ solution of 6.4−6.5.

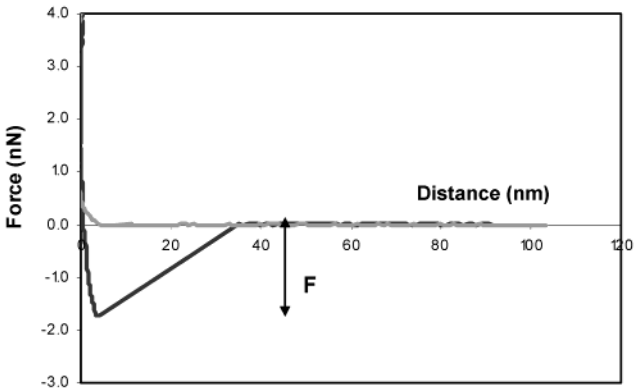

Figure 1. Typical approach (gray line) and retraction (black line) force−distance curves measured between $\alpha_5\beta_1$ integrins immobilized on an AFM tip and peptide−amphiphile bilayer membranes in 1 mM $MnCl_2$. The magnitude of the measured adhesion force is shown by the arrow. This force profile indicates that adhesion events happen on the surface without any prior molecular extensions.

To minimize the drift effects, AFM was warmed for at least 0.5 h before an experiment. AFM force data were converted to force−distance curves using the DI-AFM software (Nanoscope III).

Results and Discussion

Direct force measurements were utilized to characterize the adhesive interactions between pure $\alpha_5\beta_1$ integrins, immobilized on AFM tips, and peptide−amphiphiles that mimic the cell adhesion domain of fibronectin, assembled into monolayers via the LB technique. Collective force measurements were performed at a constant loading rate of 59.8 nN/s. A typical AFM force−distance curve is presented in Figure 1. The adhesion events reported in this study are surface adhesion events, and the arrow in Figure 1 indicates the magnitude of the adhesion force. A small portion of the force profiles showed a combination of stretching and unbinding events similar to those reported previously.[53] The adhesive interactions between $\alpha_5\beta_1$ integrins and fibronectin mimetic surfaces were studied at the collective level, when each adhesion event corresponds to the rupture of multiple biomolecular bonds.

Specificity was confirmed in two ways: by varying the ion concentration (Figure 2) and by using inactive sequences, such as the GRGESP peptide−amphiphile (Figures 4 and 7) and PEG120 (Figure 7), as negative controls. The role of divalent cations in integrin function is demonstrated by the lack of ligand binding upon removal of cations by chelating agents.[17] Furthermore, as mentioned in the Introduction, divalent cations can be used to influence integrin activity and function in vitro. The effect of Mn^{2+} and Ca^{2+} ions on the $\alpha_5\beta_1$−GRGDSP specific binding is shown in Figure 2. The same probe was used for all these measurements. This graph demonstrates an increase in adhesion in the presence of Mn^{2+} ions and a decrease in the presence of Ca^{2+} in a concentration-dependent manner. Further decrease of integrin activity is shown upon addition of the chelating agent, ethylenediaminetetraacetic acid (EDTA). To show that this effect is reversible, at the end of the experiment the AFM cell was flushed with a 5 mM $MnCl_2$ solution and the

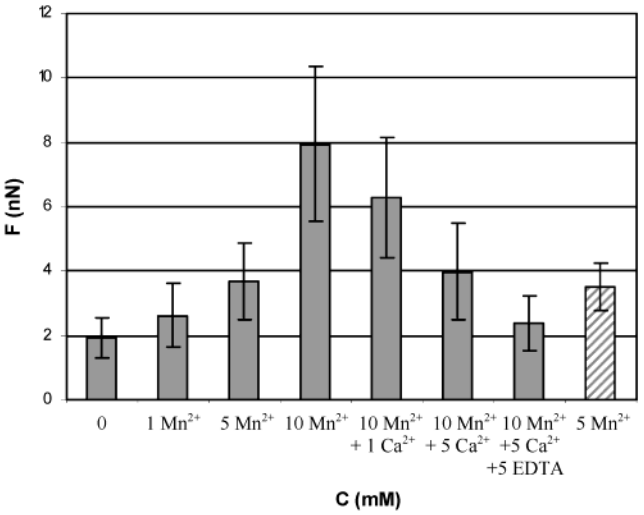

Figure 2. Effect of divalent cations on the specific binding of $\alpha_5\beta_1$−GRGDSP. The same tip was used for these measurements. Each column is the average of 25−35 measurements. The error bars show standard deviations and reflect the fact that the number of pairs that interact every time the two surfaces are brought into contact can vary from one measurement to another.

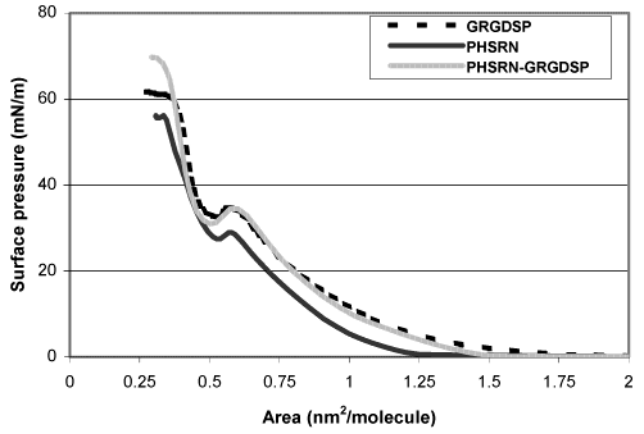

Figure 3. Surface pressure−area isotherms of PHSRN, GRGDSP, and PHSRN-GRGDSP peptide−amphiphiles on a DI water subphase at room temperature.

adhesion that was measured appeared to be of the same order of magnitude as the one measured at the beginning of the experiment for the same concentration of $MnCl_2$ solution.

To verify that peptide−amphiphiles form well-organized self-assembled monolayers that can be transferred on a solid support with minimal disruption, LB isotherms of pure peptide−amphiphiles were recorded. Figure 3 shows Langmuir isotherms of GRGDSP, PHSRN, and PHSRN-GRGDSP peptide−amphiphiles at the air−water interface. The surface pressure, which can be interpreted as a measure of the resistance of amphiphilic molecules against lateral compression, was detected at surface areas of 1.5 nm^2/molecule for pure PHSRN-GRGDSP peptide−amphiphiles. As monolayers were compressed, the surface pressure increased and at areas of 0.32−0.42 nm^2/molecule, which is consistent with closely packed tails,[60] no further compression was possible and pure monolayers collapsed at the maximum surface pressure of 61 mN/m for GRGDSP, 56 mN/m for PHSRN, and 69 mN/m for PHSRN-GRGDSP monolayers. The steep slope prior to collapse and high

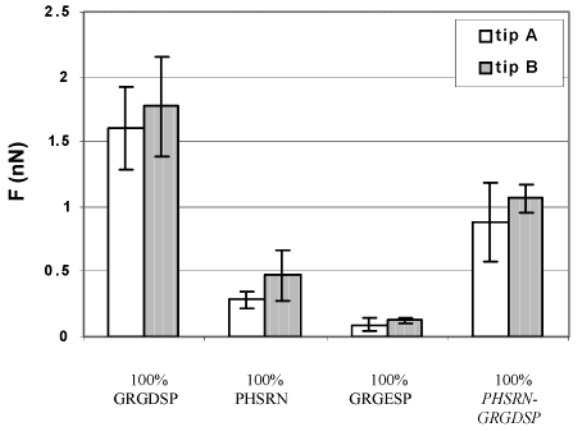

Figure 4. Adhesion measurements between immobilized $\alpha_5\beta_1$ integrins and different surfaces in a 1 mM $MnCl_2$ solution. Data correspond to the average values of 30−40 force measurements on each surface. The error bars show standard deviations and reflect the fact that the number of pairs that interact every time the two surfaces are brought into contact can vary from one measurement to another. $\alpha_5\beta_1$ integrins do not bind to the inactive GRGESP surface, which confirms their specificity for RGD-containing peptides. The binding affinity of the receptor is decreased for a surface constructed from the new PHSRN-GRGDSP peptide−amphiphile if compared to the 100% GRGDSP surface. Pure PHSRN surfaces do not show a significant adhesion.

collapse pressure indicate the presence of highly ordered and stable single monolayers, which can be transferred on a solid support with minimal disruption.

Peptide−amphiphiles with long headgroups may undergo a phase transition when compressed into monolayers at the air−water interface, which appears as a "hump" on the LB isotherm.[52] When the surface pressure is low (i.e., when there is more space per molecule), the peptide headgroup may fold onto itself, thus acquiring a bent configuration. However, as the monolayer is compressed (i.e., as the area/molecule is reduced), the headgroups are forced into a straight configuration, thus resulting in a reduction of the surface pressure. Figure 3 shows that all three peptide−amphiphiles undergo this type of transition. Thus, the ability of longer peptides to bend at lower surface pressures may be employed for exposing more of the active sequence at the interface.

Figure 4 presents force measurements between $\alpha_5\beta_1$ integrins and surfaces constructed from GRGDSP, PHSRN, GRGESP, and the new PHSRN-GRGDSP peptide−amphiphile in the 1 mM $MnCl_2$ solution at room temperature. The GRGESP peptide−amphiphile was used here as another way to verify specificity. The results show that the $\alpha_5\beta_1$ integrins bind preferentially to GRGDSP-containing peptides but not to the surfaces constructed from GRGESP amphiphiles. The results also indicate that the new sequence gives smaller adhesion compared to 100% GRGDSP.

A possible explanation of this behavior may be given after analyzing the surface pressure−area isotherm and deposition conditions of PHSRN-GRGDSP (Figure 3). We speculate that, when peptide−amphiphiles are deposited on a solid support at surface pressures above the "hump", only the tip of the peptide sequence is exposed at the interface because at high surface pressures closely packed monolayers are formed. The PHSRN-GRGDSP headgroup is long (18 amino acid residues), and when deposited at the surface pressure

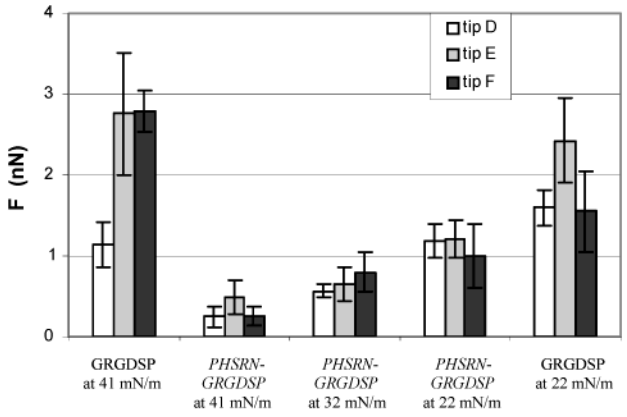

Figure 5. Effect of deposition pressure on adhesion between immobilized $\alpha_5\beta_1$ integrins and PHSRN-GRGDSP amphiphiles measured in 1 mM $MnCl_2$ solution. PHSRN-GRGDSP surfaces deposited at 22 mN/m give an increase in adhesion compared to PHSRN-GRGDSP surfaces deposited at 41 mN/m, but the strength of adhesion is still smaller than the one for the 100% GRGDSP surfaces, deposited at corresponding surface pressures.

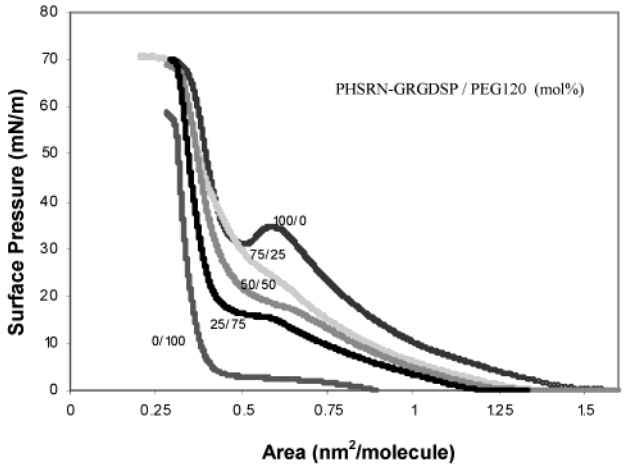

Figure 6. Surface pressure−area isotherms of mixtures of PHSRN-GRGDSP/PEG120 amphiphilic molecules on a DI water subphase at room temperature.

of 41 mN/m (the "solid" region on the LB isotherm) we hypothesize that PHSRN, the synergy sequence, is buried within the monolayers and cannot contribute to the interaction between the PHSRN-GRGDSP peptide and $\alpha_5\beta_1$ integrin. As a result, surfaces containing pure PHSRN-GRGDSP deposited at 41 mN/m give smaller adhesion compared to 100% GRGDSP surfaces (Figure 4).

Thus, to achieve an increase in adhesion between $\alpha_5\beta_1$ integrins and PHSRN-GRGDSP surfaces, we need to provide more space for the headgroups to bend and expose the bioactive peptide sequence at the interface. Two approaches were utilized in an attempt to reach this goal. In the first one, PHSRN-GRGDSP amphiphiles were deposited at lower surface pressures, 32 and 22 mN/m, which correspond to the "fluid" region on the LB isotherm for this molecule (Figure 3). These surface pressure values are on and below the "hump" on the PHSRN-GRGDSP isotherm (Figure 3), which means that some headgroups of the peptide−amphiphiles may be bent. Results of adhesion force measurements between $\alpha_5\beta_1$ integrins and 100% PHSRN-GRGDSP amphiphiles deposited at various surface pressures are shown in Figure 5. 100% GRGDSP surfaces deposited at 41 mN/m and at 22 mN/m were used to compare the performance of the new sequence. As the pressure decreased an increase in the $\alpha_5\beta_1$−PHSRN-GRGDSP adhesion was observed. PHSRN-GRGDSP surfaces deposited at 22 mN/m gave an increase in adhesion compared to PHSRN-GRGDSP surfaces deposited at 41 mN/m, but the strength of adhesion is still smaller than the one for 100% GRGDSP surfaces, deposited at corresponding surface pressures. The reason for such a result might be that the PHSRN-GRGDSP headgroups, given more space per molecule, fold or bend over adjacent molecules and a portion of the active sequence may still be buried.

To verify that lipid tails are not exposed when membranes are deposited at lower surface pressures and, thus, no additional hydrophobic interaction is contributing to the adhesion force, height analysis of the surfaces used in this experiment was performed (AFM images not shown). The results of the analysis indicate that the height variations across the PHSRN-GRGDSP surfaces are 3.043 ± 1.080 nm for a deposition pressure of 22 mN/m, 2.333 ± 0.893 nm for 32 mN/m, and 2.440 ± 0.676 nm for 41 mN/m. As expected, surfaces deposited at the lowest surface pressure of 22 mN/m have the largest height variations. However, even the maximum height difference of about 4 nm is much smaller than the length of the PHSRN-GRGDSP headgroup in a straight conformation, which is approximately 7.3 nm [18 amino acids times 0.37 nm per amino acid,[57] plus the length of the (Glu) linker and $(CH_2)_2$ spacer].[46] This implies that, when surfaces are deposited at a lower surface pressure, the dialkyl tails are not exposed at the interface. Furthermore, no holes were observed on the AFM images. Therefore, no additional hydrophobic contribution to the adhesion force is expected.

The effect of PEG120 was investigated as a second approach for providing more space for the PHSRN-GRGDSP headgroups to bend and expose the binding sequence at the interface. For this purpose, PHSRN-GRGDSP amphiphiles were mixed with PEG120 amphiphilic molecules at peptide concentrations of 25, 50, and 75 mol %. Figure 6 shows the surface pressure−area isotherms recorded at the air−water interface for mixed monolayers, as well as those for pure PEG120 and PHSRN-GRGDSP. The PEG120 headgroup length is 1.6 nm,[46] and the headgroup of the PHSRN-GRGDSP peptide−amphiphile is 7.3 nm. Because the PEG120 headgroup is smaller than that of the PHSRN-GRGDSP, the mean molecular areas measured for mixed monolayers should increase with the molar peptide concentration[61] and isotherms for mixtures should fall between the isotherms for pure PEG120 and PHSRN-GRGDSP. The collapse pressures for the pure PHSRN-GRGDSP monolayer and its mixtures with PEG120 are about 70 mN/m and, for PEG120, 58 mN/m. These data along with the steep slope prior to collapse indicate that PHSRN-GRGDSP peptide−amphiphiles, lipidated PEG (DSPE-PEG120), and their mixtures possess good assembly properties and arrange themselves into highly organized and stable monolayers upon compression. Therefore, these monolayers can be deposited on a solid support with minimal disruption.

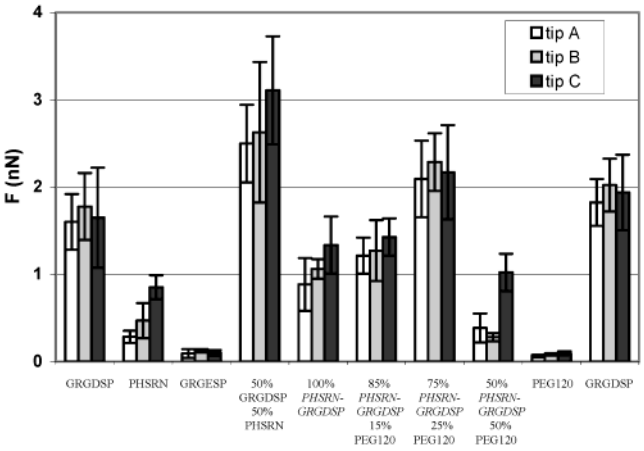

Figure 7. Adhesion measurements between immobilized $\alpha_5\beta_1$ integrins and different surfaces in 1 mM $MnCl_2$ solution. Each column is an average of 30−40 measurements on each surface. The error bars show standard deviations and reflect the fact that the number of pairs that interact may vary from one measurement to another. $\alpha_5\beta_1$ integrins do not bind to the PEG120 and GRGESP surfaces. PHSRN surfaces give smaller adhesion compared to GRGDSP. Mixtures of 75:25% PHSRN-GRGDSP/PEG120 give an increase in adhesion compared to pure PHSRN-GRGDSP and a comparable adhesion to surfaces with pure GRGDSP or 50:50% GRGDSP/PHSRN.

Figure 7 presents force measurements between $\alpha_5\beta_1$ integrins and different LB membranes. As discussed previously, PEG120 has a much shorter headgroup compared to the PHSRN-GRGDSP headgroup and, thus, was used as an effective way to provide more space for the PHSRN-GRGDSP to bend and expose more of the active sequence at the interface. AFM images of the surfaces (data not shown) revealed that mixtures at 25:75 mol % PHSRN-GRGDSP/PEG120 phase-separated and, thus, were excluded from the adhesion measurement experiments. Our results demonstrate that $\alpha_5\beta_1$ integrins do not bind to PEG120 and GRGESP amphiphiles (Figure 7), which confirms specificity. PHSRN surfaces give smaller adhesion compared to GRGDSP. In PHSRN-GRGDSP/PEG120 mixtures, an increase in adhesion is observed as the PEG120 concentration is increased up to 25 mol % compared to 100% PHSRN-GRGDSP. This result verifies our hypothesis that decreased adhesion for 100% PHSRN-GRGDSP surfaces was observed because PHSRN was partially buried within the monolayer. Thus, mixtures of 75:25 mol % PHSRN-GRGDSP/PEG120 give an increase in adhesion compared to 100% PHSRN-GRGDSP and comparable adhesion to surfaces with pure GRGDSP or 50:50 mol % GRGDSP/PHSRN. AFM images (not shown) of the 50:50 mixture of GRGDSP and PHSRN were taken to verify that the two peptides are well mixed, and phase separation is not observed. To show that the integrins do not lose their activity during the measurements, at the end of the experiment adhesion forces were measured with GRGDSP surfaces and the adhesion force appeared to be of the same order of magnitude as the one measured at the beginning of the experiment for GRGDSP surfaces.

Surfaces constructed from 50:50 mol % GRGDSP/PHSRN give slightly higher adhesion compared to 75:25 mol % PHSRN-GRGDSP/PEG120. The reason for such a result may be that some PHSRN sites in our new PHSRN-GRGDSP sequence may still be partially buried within the 75:25% monolayer of PHSRN-GRGDSP/PEG120 and may not be fully exposed at the interface. Moreover, the linker between PHSRN and GRGDSP, $(SG)_3S$, may not be the optimal one and needs further improvements. Currently, work is being done to optimize the new sequence taking into account these two considerations.

It would be desirable to be able to identify the number of individual bonds involved in each adhesion event. However, this is not trivial. One would need to know the geometry of the system, that is, the exact radius of the AFM tip, and the percentage of integrin surface coverage for every tip. Unfortunately, the exact radius of the AFM tip is not known and can vary from 5 to 40 nm according to specifications of the manufacturer, and there is no easy way to calculate the integrin surface coverage for every AFM tip considering its small radius. Thus, a more reliable way to determine the number of individual bonds involved in each adhesion event would be to perform single-molecule force spectroscopy and to identify the force quantum for a single receptor−ligand pair. At this point, we have accurately determined the force quantum for the GRGDSP−$\alpha_5\beta_1$ pair to be 22 ± 3 pN at a loading rate of 59 nN/s.[53] Therefore, on the basis of adhesion forces presented at the beginning of the experiment in Figure 7, 73 ± 18 individual bonds can be correlated to the adhesion force measured between $\alpha_5\beta_1$−GRGDSP using tip A, 81 ± 21 using tip B, and 75 ± 28 using tip C. However, we cannot assume that the same number of receptors are involved in interactions with every surface in Figure 7. Work is currently in progress to determine the force quantum for the PHSRN-GRDGSP−$\alpha_5\beta_1$ pair and, thus, to correlate the number of individual biomolecular bonds to the adhesion force measured at the collective level.

Conclusions

In this study, we have attempted to develop a way to create a biologically active membranelike surface that mimics the cell-adhesion domain of fibronectin, in which ligand composition and accessibility were used as means to control interaction with immobilized integrins. For this, a peptide−amphiphile $(C_{16})_2$-Glu-C_2-PHSRN$(SG)_3$SGRGDSP was designed and characterized that contains both the primary recognition sequence for $\alpha_5\beta_1$ integrins, GRGDSP, and the synergy sequence, PHSRN. The focus of this study was to design and test a linker that would most closely mimic the distance and the nature of the space between PHSRN and GRGDSP sequences in the fibronectin molecule. Thus, the $(SG)_3S$ amino acid combination was used to link the two bioactive sequences in a single linear peptide formulation, which mimics the hydrophobic−hydrophilic nature and the 30−40 Å separation distance between the two sequences in fibronectin.

The specificity of the $\alpha_5\beta_1$ integrin for the GRGDSP ligand was established by varying the concentration of divalent cations and using an inactive peptide−amphiphile (GRGESP) and PEG120 as negative controls. It was shown that, as in the case when integrins are incorporated into a cell membrane, Mn^{2+} increased and Ca^{2+} decreased the adhesion of the immobilized $\alpha_5\beta_1$ to GRGDSP amphiphiles and adding

a chelating agent, EDTA, further reduced integrin activity. $\alpha_5\beta_1$ integrins did not bind to surfaces constructed from either GRGESP or PEG120.

The new sequence, PHSRN-GRGDSP, gives an increase in $\alpha_5\beta_1$ adhesion when compared to pure GRGDSP. This increase in adhesion was observed when 75 mol % of PHSRN-GRGDSP amphiphiles were mixed with 25 mol % of a short amphiphilic molecule (lipidated PEG120), which was used to provide more space for peptide−amphiphiles to bend and expose more of the active sequence at the interface. This result demonstrates that accessibility of the PHSRN sequence is crucial in designing fibronectin-mimetic surfaces and can be used as means to control interaction with integrins. Thus, to achieve the highest synergistic effect with a biomimetic surface it is essential that both GRGDSP and PHSRN sequences are presented at the interface in appropriate spatial orientation and that both of them are accessible to a single integrin receptor.

The new sequence gives comparable adhesion to surfaces containing 50 mol % GRGDSP and 50 mol % PHSRN. To maximize the $\alpha_5\beta_1$ adhesion, the new sequence needs further improvement, and currently work is being done to optimize the sequence and its presentation at the interface.

In summary, when surfaces are functionalized with biomacromolecules that mimic the adhesion domain of fibronectin protein the synergy site of the protein is required for increased adhesion, and this synergistic effect strongly depends on its accessibility to the receptor.

Acknowledgment. Partial financial support from MRSEC at the University of Massachusetts, Amherst, under NSF DMR 021 3695 is gratefully acknowledged. Acknowledgment is also made to the Donors of the American Chemical Society Petroleum Research Fund, for partial support of this research.

References and Notes

(1) Hammer, D. A.; Tirrell, M. *Annu. Rev. Mater. Sci.* **1996**, *26*, 651−691.
(2) Fletcher, M. Bacterial attachment in aquatic environment: a diversity of surfaces and adhesion strategies. In *Bacterial Adhesion: Molecular and Ecological Diversity*; Fletcher, M., Ed.; John Wiley and Sons: New York, 1996.
(3) Lauffenburger, D. A.; Horwitz, A. F. *Cell* **1996**, *84*, 359−369.
(4) DiMilla, P. A.; Barbee, K.; Lauffenburger, D. A. *Biophys. J.* **1991**, *60*, 15−37.
(5) DiMilla, P. A.; Stone, J. A.; Quinn, J. A.; Albelda, S. M.; Lauffenburger, D. A. *J. Cell Biol*. **1993**, *122*, 729−737.
(6) Goodman, S. L.; Risse, G.; von der Mark, K. *J. Cell Biol*. **1989**, *109*, 799−809.
(7) Huttenlocher, A.; Ginsberg, M. H.; Horwitz, A. F. *J. Cell Biol*. **1996**, *134*, 1551−1562.
(8) Maheshwari, G.; Wells, A.; Griffith, L. G.; Lauffenburger, D. A. *Biophys. J*. **1999**, *76*, 2814−2823.
(9) Palecek, S. P.; Loftus, J. C.; Ginsberg, M. H.; Lauffenburger, D. A.; Horwitz, A. F. *Nature* **1997**, *385*, 537−540.
(10) Wu, P.; Hoying, J. B.; Williams, S. K.; Kozikowski, B. A.; Lauffenburger, D. A. *Ann. Biomed. Eng*. **1994**, *22*, 144−152.
(11) Coe, A. P.; Askari, J. A.; Kline, A. D.; Robinson, M. K.; Kirby, H.; Stephens, P. E.; Humphries, M. J. *J. Biol. Chem.* **2001**, *276*, 35854−35866.
(12) Mould, A. P.; Askari, J. A.; Aota, S.; Yamada, K. M.; Irie, A.; Takada, Y.; Mardon, H. J.; Humphries, M. J. *J. Biol. Chem*. **1997**, *272*, 17283−17292.
(13) Xiong, J. P.; Stehle, T.; Diefenbach, B.; Zhang, R.; Dunker, R.; Scott, D. L.; Joachimiak, A.; Goodman, S. L.; Arnaout, M. A. *Science* **2001**, *294*, 339−345.
(14) Arroyo, A. G.; Garcia-Pardo, A.; Sanchez-Madrid, F. *J. Biol. Chem*. **1993**, *268*, 9863−9868.
(15) Tsuchida, J.; Ueki, S.; Takada, Y.; Saito, Y.; Takagi, J. *J. Cell Sci.* **1998**, *111*, 1759−1766.
(16) Fernandez, C.; Clark, K.; Burrows, L.; Shofield, N. R.; Humphries, M. J. *Front. Biosci*. **1998**, *3*, d684−d700.
(17) Mould, A. P.; Akiama, S. K.; Hamphries, M. J. *J. Biol. Chem*. **1995**, *270*, 26270−26277.
(18) Kuo, S. C.; Lauffenburger, D. A. *Biophys. J*. **1993**, *65*, 2191−2200.
(19) Ruoslahti, E. *Annu. Rev. Cell Dev. Biol.* **1996**, *12*, 697−715.
(20) Yamada, K. *J. Biol. Chem*. **1991**, *266*, 12809−12812.
(21) Johansson, S.; Svineng, G.; Wennerberg, K.; Armulik, A.; Lohikangas, L. *Front. Biosci*. **1997**, *2*, d126−d146.
(22) Ruoslahti, E.; Reed, J. *Nature* **1999**, *397*, 479−480.
(23) Massia, S. P.; Hubbell, J. A. *J. Cell Biol*. **1991**, *114*, 1089−1100.
(24) Massia, S. P.; Stark, J. *J. Biomed. Mater. Res*. **2001**, *56*, 390−399.
(25) Cook, A. D.; Hrkach, J. S.; Nicholas, N. G.; Johnson, I. M.; Pajvani, U. B.; Cannizzaro, S. M.; Langer, R. *J. Biomed. Mater. Res.* **1997**, *35*, 513−523.
(26) Kugo, K.; Okuno, M.; Masuda, K.; Nishino, J.; Masuda, H.; Iwatsuki, M. *J. Biomater. Sci., Polym. Ed*. **1994**, *5*, 325−337.
(27) Neff, J. A.; Tresco, P. A.; Caldwell, K. D. *Biomaterials* **1999**, *20*, 2377−2393.
(28) Hubbell, J. L. *Curr. Opin. Biotechnol*. **1999**, *10*, 123−129.
(29) Barerra, D. A.; Zylstra, E.; Landsbury, P. T.; Langer, R. *J. Am. Chem. Soc*. **1993**, *115*, 11010−11011.
(30) Porte-Durieu, M. C.; Labrugere, C.; Villars, F.; Lefebvre, F.; Dutoya, S.; Guette, A.; Bordenave, L.; Baquey, C. *J. Biomed. Mater. Res*. **1999**, *46*, 368−375.
(31) Rezania, A.; Thomas, C. H.; Branger, A. B.; Waters, C. M.; Healy, K. E. *J. Biomed. Mater. Res*. **1997**, *37*, 9−19.
(32) Glass, J. R.; Dickerson, K. T.; Stecker, K.; Polarek, J. W. *Biomaterials* **1996**, *17*, 1101−1108.
(33) Hern, D. L.; Hubbell, J. A. *J. Biomed. Mater. Res*. **1998**, *39*, 266−276.
(34) Zhang, S. G.; Yan, L.; Altman, M.; Lassle, M.; Nuggent, H.; Frankel, F.; Lauffenburger, D. A.; Whitesides, G. M.; Rich, A. *Biomaterials* **1999**, *20*, 1213−1220.
(35) Lahiri, J.; Ostuni, E.; Whitesides, G. M. *Langmuir* **1999**, *15*, 2055−2060.
(36) Roberts, C.; Chen, C. S.; Mrksich, M.; Martichonok, V.; Ingber, D. E.; Whitesides, G. M. *J. Am. Chem. Soc*. **1998**, *120*, 6548−6555.
(37) Kokkoli, E.; Tirrell, M.; Biesalski, M. *Surf. Sci.* **2002**, *500*, 61−83.
(38) Berndt, P.; Fields, G. B.; Tirrell, M. *J. Am. Chem. Soc*. **1995**, *117*, 9515−9522.
(39) Winger, T. M.; Ludovice, P. J.; Chaikof, E. L. *Biomaterials* **1996**, *17*, 437−441.
(40) Yu, Y.-C.; Berndt, P.; Tirrell, M.; Fields, G. B. *J. Am. Chem. Soc*. **1996**, *118*, 12515−12520.
(41) Yu, Y.-C.; Pakalns, T.; Dori, Y.; McCarthy, J. B.; Tirrell, M.; Fields, G. B. *Methods Enzymol*. **1997**, *289*, 571−587.
(42) Yu, Y.-C.; Tirrell, M.; Fields, G. B. *J. Am. Chem. Soc*. **1998**, *120*, 9979−9987.
(43) Fields, G. B.; Lauer, J. L.; Dori, Y.; Forns, P.; Yu, Y.-C.; Tirrell, M. *Biopolymers* **1998**, *47*, 143−151.
(44) Schneider, J.; Berndt, P.; Haverstick, K.; Kumar, S.; Chiruvolu, S.; Tirrell, M. *Langmuir* **2002**, *18*, 3923−3931.
(45) Pakalns, T.; Haverstick, K. L.; Fields, G. B.; McCarthy, J. B.; Mooradian, D. L.; Tirrell, M. *Biomaterials* **1999**, *20*, 2265−2279.
(46) Dori, Y.; Bianco-Peled, H.; Satija, S. K.; Fields, G. B.; McCarthy, J. B.; Tirrell, M. *J. Biomed. Mater. Res.* **2000**, *50*, 75−81.
(47) Lasic, D., Martin, F., Eds. *Stealth liposomes*; CRC Press: Boca Raton, FL, 1995.
(48) Leahy, D. J.; Aukhil, I.; Erickson, H. P. *Cell* **1996**, *84*, 155−164.
(49) Hynes, R. O. *Fibronectins*; Springer-Verlag: New York, 1990.
(50) Kenneth, Y. M. *J. Clin. Invest.* **2000**, *105*, 1507−1509.
(51) Francis, S. E.; Goh, K. L.; Hodivala-Dilke, K.; Bader, B. L.; Stark, M.; Davidson, D.; Hynes, R. O. *Arterioscler., Thromb., Vasc. Biol*. **2002**, *22*, 927−933.
(52) Dillow, A. K.; Ochsenhirt, S. E.; McCarthy, J. B.; Fields, G. B.; Tirrell, M. *Biomaterials* **2001**, *22*, 1493−1505.
(53) Kokkoli, E.; Ochsenhirt, S. E.; Tirrell, M. *Langmuir* **2004**, in press.
(54) Kao, W. J.; Lee, D.; Schense, J. C.; Hubbell, J. A. *J. Biomed. Mater. Res.* **2001**, *55*, 79−88.
(55) Hojo, K.; Suzuki, Y.; Maeda, M.; Okazaki, I.; Nomizu, M.; Kamada, H.; Yamamoto, Y.; Nakagawa, S.; Mayumi, T.; Kawasaki, K. *Bioorg. Med. Chem. Lett.* **2001**, *11*, 1429−1432.
(56) Aucoin, L.; Griffith, C. M.; Pleizier, G.; Deslandes, Y.; Sheardown, H. *J. Biomater. Sci., Polymer Ed*. **2002**, *13*, 447−462.

(57) Idiris, A.; Alam, M. T.; Ikai, A. *Protein Eng.* **2000**, *13*, 763−770.
(58) Hansma, H. G.; Clegg, D. O.; Kokkoli, E.; Oroudjev, E.; Tirrell, M. *Methodol. Cell Biol.* **2002**, *69*, 163−193.
(59) Burnham, N. A.; Behrend, O. P.; Oulevey, F.; Gremaud, G.; Gallo, P.-J.; Gourdon, D.; Dupas, E.; Kulik, A. J.; Pollock, H. M.; Briggs, G. A. D. *Nanotechnology* **1997**, *8*, 67−75.
(60) Tanford, C. *The hydrophobic effect: formation of micelles and biological membranes*; Wiley: New York, 1980.
(61) Dufrene, Y. F.; Barger, W. R.; Green, J.-B. D.; Lee, G. U. *Langmuir* **1997**, *13*, 4779−4784.

BM0344351